Research

Author for correspondence:
Roy A. Quinlan
email: r.a.quinlan@durham.ac.uk

†These authors contributed equally to this study.

Royal Society **Publishing**
Informing the science of the future

The specificity of the interaction between αB-crystallin and desmin filaments and its impact on filament aggregation and cell viability

Jayne L. Elliott[1,2,†], Ming Der Perng[1,3,†], Alan R. Prescott[4], Karin A. Jansen[5], Gijsje H. Koenderink[5] and Roy A. Quinlan[1,2]

[1]School of Biological and Biomedical Sciences, and [2]Biophysical Sciences Institute, The University of Durham, South Road, Durham DH1 3LE, UK
[3]Institute of Molecular Medicine, College of Life Sciences, National Tsing Hua University, Hsinchu 300, Taiwan, Republic of China
[4]CHIPs and Division of Cell Signalling and Immunology, College of Life Sciences, University of Dundee, WTB/MSI complex, Dundee DD1 5EH, UK
[5]FOM Institute AMOLF, Science Park 104, Amsterdam XG 1098, The Netherlands

CRYAB (αB-crystallin) is expressed in many tissues and yet the R120G mutation in CRYAB causes tissue-specific pathologies, namely cardiomyopathy and cataract. Here, we present evidence to demonstrate that there is a specific functional interaction of CRYAB with desmin intermediate filaments that predisposes myocytes to disease caused by the R120G mutation. We use a variety of biochemical and biophysical techniques to show that plant, animal and ascidian small heat-shock proteins (sHSPs) can interact with intermediate filaments. Nevertheless, the mutation R120G in CRYAB does specifically change that interaction when compared with equivalent substitutions in HSP27 (R140G) and into the *Caenorhabditis elegans* HSP16.2 (R95G). By transient transfection, we show that R120G CRYAB specifically promotes intermediate filament aggregation in MCF7 cells. The transient transfection of R120G CRYAB alone has no significant effect upon cell viability, although bundling of the endogenous intermediate filament network occurs and the mitochondria are concentrated into the perinuclear region. The combination of R120G CRYAB co-transfected with wild-type desmin, however, causes a significant reduction in cell viability. Therefore, we suggest that while there is an innate ability of sHSPs to interact with and to bind to intermediate filaments, it is the specific combination of desmin and CRYAB that compromises cell viability and this is potentially the key to the muscle pathology caused by the R120G CRYAB.

1. Introduction

The discovery that the R120G mutation in αB-crystallin (CRYAB, HSPB5 [1]) phenocopies desmin mutations [2,3] in human desmin-related myopathies (DRMs) provided the first genetic evidence in support of the proposed functional interaction between CRYAB and intermediate filaments [4]. Since that discovery, there have been many studies on the mechanisms that cause DRM. These have included the identification of the amyloid-forming potential of CRYAB [5,6], the involvement of the proteosomal [7] and macroautophagy pathways [8], as well as the propagation of apoptotic signals via desmin fragmentation [9] and the involvement of mitochondria [10]. Desmin is intimately involved in mitochondrial positioning and homeostasis [11–15] and mitochondrial changes are a prominent associated phenotype in both DRM patients [16] and mouse models of cardiomyopathy [17]. The caspase 6-mediated fragmentation of desmin produces an *N*-terminal fragment that promotes filament aggregation [9]. Blocking this has been shown to attenuate another model of

cardiomyopathy based on tumour necrosis factor-mediated apoptosis [18]. Other mouse models of cardiomyopathy that have not genetically targeted desmin or CRYAB expression [19,20] see changes in desmin distribution and its inclusion into aggregates and an association with CRYAB. The emerging consensus is that the redistribution of desmin into aggregates [21,22] is a key initiator in the pathology of DRMs.

Protein aggregates containing both desmin and CRYAB were a feature of the description of the R120G CRYAB family [1]. This was faithfully replicated in a knock-in mouse model of the R120G CRYAB disease-causing mutation, with desmin aggregation in muscles and the additional observation of increased vimentin aggregation in the lenses of these animals [23]. Cataracts were also noted in those family members expressing R120G CRYAB [1]. These data could suggest that the CRYAB interaction may not be specific to desmin, as vimentin also associates with CRYAB [4]. Indeed, the co-association of CRYAB with intermediate filament aggregates is a common histopathological feature in the human diseases caused by mutant cytoplasmic intermediate filament proteins that form aggregates [24]. Therefore, it is important to examine the specificity of the functional interaction between desmin filaments and CRYAB if we are to understand fully the muscle pathology caused by mutant CRYAB and desmin.

Previously, we have shown that small heat-shock proteins (sHSPs) are important modulators of intermediate filament assemblies [4]. They can prevent filament–filament interactions from occuring on the basis of an *in vitro*-based viscosity assay and transient transfection studies [25]. The R120G mutation in CRYAB was found to abrogate this activity both for glial fibrillary acidic protein (GFAP) [25] and desmin filaments [26], promoting instead filament–filament interactions and their aggregation. Mutations in other sHSPs also cause human diseases from cataract to distal neuropathies, which include CRYAA (HSPB4), HSP27 (HSPB1), HSP27L (HSPB3; [27]) and HSP22 (HSPB8) (summarized in [28]). Intermediate filament aggregates feature in the histopathologies of such diseases, demonstrating that the interaction between sHSPs and intermediate filaments is a widespread and functionally important interaction. The question to emerge from these studies is why only certain cell types and tissues are affected by mutations in an sHSP, whereas their tissue expression profile is not usually restricted (except perhaps CRYAA [29]). CRYAB [30], HSP27 and HSP22 are all expressed in muscle [31–33], but mutations in HSP27 and HSP22 are not associated with muscle pathology.

There have been many suggestions to explain the tissue-specific pathologies associated with sHSP mutations [34–40], but we propose that the specific intermediate filament expression pattern must be considered as a key factor in any sHSP-based pathology as we consider the intermediate filament–sHSP complex to be a functional unit [41,42]. Intermediate filament expression profiles follow tissue-specific patterns according to embryological origins [43]. It has already been shown that R120G CRYAB induces the aggregation of desmin filaments [26], but it can also potentially cause the aggregation of GFAP filaments [25]. The reported pathologies for CRYAB mutations are, however, myopathies and cataract and not neuropathies. Desmin is a type III intermediate filament protein expressed in muscle, which suggests that the interaction of desmin with CRYAB is key to understanding DRM.

To test this hypothesis, we considered the consequences of introducing CRYAB R120G equivalent mutations into other sHSPs, such as HSP27 and HSP16.2, to see if equivalent mutations would also change their interaction with desmin. The R120G mutation in the α-crystallin domain of CRYAB is predicted to have similar structural consequences for HSP27 [44], and therefore for both HSP27 and CRYAB the equivalent mutation should have similar effects. We find that only the R120G CRYAB mutation induces increased binding to desmin as assessed by *in vitro* sedimentation assay. We assessed the interaction of desmin and CRYAB using a range of *in vitro* techniques (falling ball assay, Ostwald viscometry, surface plasmon resonance (SPR) and optical trap measurement of filament network elasticity) to evidence the interaction of CRYAB with desmin. We show that the binding of CRYAB to desmin is pH- and cation-dependent. Using transient transfection, we show that only the desmin-CRYAB R120G combination-induced desmin aggregates coincided with reduced cell viability in MCF7 cells. We suggest that it is the partnership of the sHSP with the resident intermediate filaments that determines how cells respond to the presence of mutant CRYAB.

2. Material and methods

(a) Expression constructs for recombinant sHSPs

Wild-type (WT) or R120G CRYAB expression vectors based on the pET23b plasmid were constructed as described previously [25]. HSP27 and R140G HSP27 were constructed as described [45]. The *Caenorhabditis elegans* HSP16.2 cDNA was cloned into the pRSET expression vector (Invitrogen) as described previously [46] using the QuickChange site-directed mutagenesis kit (Stratagene) to introduce the R95G mutation into WT HSP16.2. For live cell imaging experiments, CRYAB or desmin were subcloned into the modified pcDNA3.1 (+) vector with DsRed2-Mito (Clontech) preceded by an internal ribosomal entry site (IRES). These two vector components were PCR amplified from the vectors DsRed2-Mito (Clontech) and pWPI (http://tronolab.epfl.ch) and sequenced in pGEM-T Easy (Promega, UK) before assembling with the relevant CRYAB or desmin fragments from the pET23. These IRES-containing bicistronic vectors allow simultaneous expression of both mitochondrially targeted red fluorescent protein to indicate transfected cells and either CRYAB or desmin constructs.

(b) Expression and purification of recombinant wild-type and mutant sHSPs

Both WT and mutant sHSPs were expressed in and purified from BL21(DE3) pLysS *Escherichia coli* as described. WT and R120G CRYAB were purified as described using two diethylaminoethanol (DEAE) column steps at 4°C [25]. Recombinant human WT and R140G HSP27 were purified using similar procedures. For further studies, purified sHSPs were refolded by dialysis against 20 mM Tris–HCl, pH 7.4, 100 mM NaCl at 4°C for 16 h.

Both the WT and R95G HSP16.2 formed inclusion bodies, which were purified [47] and then solubilized in TEN buffer containing 8 M urea. Purification required anion exchange chromatography using DEAE-cellulose (DE52; Whatman, UK) in the presence of 6 M urea. Peak fractions were pooled and then dialysed against buffer containing 20 mM Tris–HCl, pH 7.4, 100 mM NaCl. The native complex was further purified by size exclusion chromatography (SEC) on a Fractogel EMD BioSEC Superformance column (60 × 1.6 cm; Merck, UK) in the same buffer. Purified proteins were concentrated to 1 mg ml^{-1} using Ultrafree-15 (Millipore, UK) concentrators with a 10 kDa molecular weight cut-off.

(c) Preparation of desmin, glial fibrillary acidic protein and keratins

Purified desmin was obtained by extraction of the crude intermediate filament preparation from chicken gizzards with 8 M urea and the subsequent chromatography on DEAE-cellulose and hydroxyapitite columns in the presence of 6 M urea as described previously [48,49]. Recombinant human desmin, GFAP, keratins 7 and 18 were purified as described [4,26,50,51]. Protein concentrations were determined by the bicinchonic acid assay (BCA reagent, Pierce) using bovine serum albumin as standard.

(d) Size exclusion chromatography of sHSPs

Molecular size of the recombinant sHSP complexes were measured by gel filtration chromatography on a Superformance column (60 × 1.6 cm) packed with Fractogel EMD BioSEC (Merck, UK). The column was calibrated using thyroglobulin (669 kDa), apoferritin (440 kDa), alpha-amylase (200 kDa), bovine serum albumin (67 kDa) and carbonic anhydrase (29 kDa). The column void volume was determined using dextran blue (2000 kDa). Proteins were eluted in buffer containing 20 mM Tris–HCl, pH 7.4 and 100 mM NaCl at room temperature and the elution volume of each sample was used to estimate the molecular weight.

(e) Intermediate filament assembly, binding and viscosity assays involving sHSPs

Low-speed and high-speed sedimentation assays were used to assess the ability of sHSPs to associate with intermediate filaments and prevent filament–filament associations that lead to aggregation [52]. Intermediate filament proteins were mixed with sHSPs in urea buffer (8 M urea, 20 mM Tris–HCl, pH 8.0, 5 mM EDTA, 2 mM EGTA, 1 mM DTT) and then dialysed to lower the urea concentration stepwise into low ionic strength buffer (10 mM Tris–HCl pH 7.0, 1 mM DTT) at 4°C. Sometimes CRYAB was added at this stage prior to initiating filament assembly by dialysis into filament assembly buffer (10 mM Tris–HCl pH 7.0, 1 mM DTT 50 mM NaCl) at room temperature for 12 h. Assembly of desmin and GFAP filaments was also initiated by the addition of a 20-fold concentrated binding buffer to low ionic strength buffer, giving a final concentration of 100 mM imidazole-HCl, pH 6.8, 1 mM DTT. Protein samples were incubated for 2 h at the indicated temperatures. Experiments to investigate pH and temperature effects on CRYAB associations were carried out as follows with WT GFAP, vimentin and desmin assembled at 0.2 mg ml^{-1} and mixed with WT CRYAB at a 1:1 molar ratio. Filament assembly was completed by dialysis into 20 mM N-2-hydroxyethylpiperazine-N-2-ethanesulfonic acid (HEPES), 100 mM NaCl, 1 mM MgCl$_2$, 1 mM DTT at pH 6.3, 6.8 or 7.3; at 23°C, 39°C or 44°C, respectively. In some instances, CRYAB was also added to assembled filaments.

The influence of sHSPs on filament–filament interactions of assembled desmin was assessed also by measuring the visco-elastic properties. First, we used a falling ball assay as described previously [51]. The ability of the sample to support a ball bearing was then scored in a binary fashion. Carbonic anhydrase (Sigma, UK) was used as a control. We performed viscosity measurements using an Ostwald-type viscometer (Cannon, USA) at a protein concentration of 0.5 mg ml^{-1} at 37°C. GFAP was assembled in the absence or the presence of CRYAB by addition of a 20-fold binding buffer as described above. Flow times were measured at different time points: 1 min after assembly start and then every 5 min over a period of 1 h. Specific viscosity (V_{sp}) was calculated by the equation $V_{sp} = (T_s - T_b)/T_b$, where T_s is the flow time of the sample and T_b the flow time of the buffer.

(f) Passive microrheology measurements

Desmin filaments were assembled from purified recombinant protein at 1 mg ml^{-1} with or without a 1:10 molar ratio of desmin : CRYAB using dialysis to lower the urea concentration. Assembly was completed by overnight dialysis into 20 mM Tris–HCl (pH 7.3), 50 mM NaCl, 1 mM MgCl$_2$ and 1 mM DTT at room temperature. One-particle passive microrheology was done using a 808 nm laser and a 100× oil objective (NA 1.4) on an inverted Nikon phase microscope. PLL-coated polystyrene beads of 1.5 µm were trapped, laser light was collected using an oil condenser, and the intensity fluctuations were recorded using a quadrant photodiode (QPD). With a custom-written program in C++, the apparent elastic modulus G'_{app} and apparent viscous modulus G''_{app} were determined from the fluctuations in bead position using the fluctuation–dissipation theorem and generalized Stokes–Einstein equation [53]. The viscous modulus was calculated from G''_{app} by subtracting the solvent viscosity, and the elastic modulus was calculated from G'_{app} by subtracting the apparent modulus in buffer to compensate for the presence of the optical trap [54].

(g) Binding of CRYAB and R120G CRYAB measured by surface plasmon resonance

Affinities of WT or R120G CRYAB to immobilized intermediate filament proteins were determined using SPR analysis with a Biacore 3000 apparatus (GE Healthcare, Uppsala, Sweden). Purified desmin, GFAP and vimentin were immobilized on the dextran matrix of a CM5 sensor chip according to the manufacturer's instructions using 10 mM HEPES, pH 7.4, 0.15 M NaCl, 3.4 mM EDTA, 0.005 % (v/v) surfactant P20. Unreacted groups were subsequently blocked by injection of 1 M ethanolamine, pH 8.5. WT and R120G CRYAB for binding to immobilized intermediate filament proteins were first diluted to 20 g ml^{-1}, injected at a flow rate of 5 l min^{-1} for 7 min at 37°C and then washed for 7 min. All sensograms were corrected for non-specific interactions to a reference surface and by double referencing [55]. The sensor chip was regenerated between injections by washing with 6 M guanidine hydrochloride in HBS-EP buffer.

(h) Cell cultures, transient transfection and cell viability assays

The immortalized human lens epithelial cell line H36CE2 was grown as detailed previously [56]. Baby hamster kidney (BHK21) cells, mouse myoblast C2C12 cells and human breast cancer epithelial cell MCF7 were grown in media as recommended by the ECACC (www.ecacc.org.uk). For co-transfection experiments, plasmid DNA (pcDNA3.1; Invitrogen, UK) containing human desmin, CRYAB, HSP27 or HSP16.2 in pcDNA3.1 (Invitrogen, UK) were prepared using MaxiPrep kits (Qiagen, UK). H36CE2 cells were transiently co-transfected by calcium phosphate precipitation using standard procedures [57], while GeneJuice Transfection Reagent (Merck Millipore, UK) was used to transiently transfect the other cell lines. Cells were allowed to recover for 24–48 h prior to processing for immunofluorescence microscopy as described previously [58]. Quantification of the desmin filament phenotypes was performed by visual assessment of various staining patterns in transfected cells. For each DNA construct, cells on three cover-slips were counted and approximately 100–150 transfected cells were assessed per coverslip. For cell viability assay, the colorimetric CellTiter 96 AQueous One Solution Cell Proliferation Assay (Promega, UK) was used according to the manufacturer's instructions. Statistical significance was analysed by one-way ANOVA and the level of significance was set at $p \leq 0.05$. Apoptotic cells were assessed by staining with a monoclonal antibody
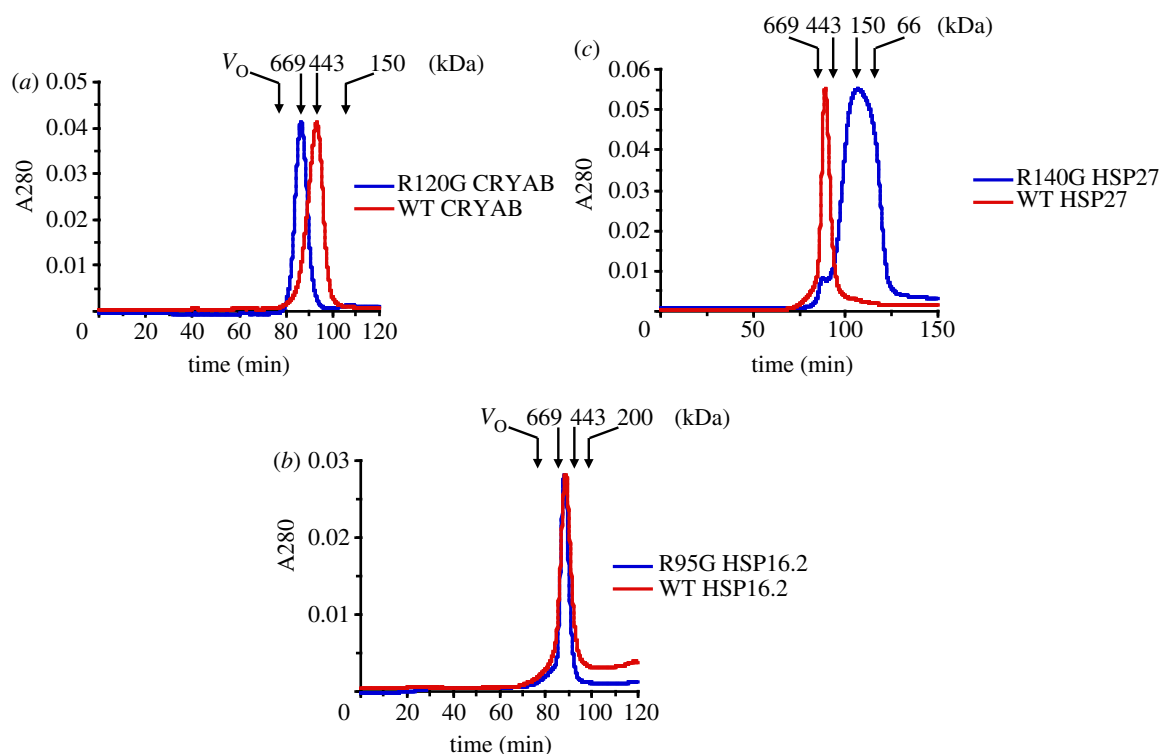
Figure 1. Analysis of oligomeric sizes of WT and mutant sHSPs. SEC was performed using a Superformance column as described in §2d. The elution profiles of WT and mutant (a) CRYAB, (b) HSP27 and (c) HSP16.2 are shown and represent an average of three independent experiments. Elution positions of molecular weight protein standards and their corresponding sizes are indicated on the top of each panel (downward arrows). The position of void volume (V_o) was determined using blue dextran. (Online version in colour.)

M30 (1 : 10, Roche Diagnostics, Mannheim, Germany) that specifically recognizes a neo-epitope of keratin 18 fragment generated by caspase cleavage at position Asp^{396} and counterstained with 5 μg ml^{-1} DAPI (Molecular Probe Inc., Eugene, OR, USA).

(i) Primary antibodies

The primary antibodies used in this study were rabbit polyclonal anti-desmin (1 : 100; Sigma, UK), desmin monoclonal (D3; Developmental Biology Hybridoma Service), mouse monoclonal anti-HSP27 (1 : 100; [59]), mouse monoclonal anti-CRYAB (1 : 1; [60]) or mouse polyclonal anti-HSP16.2 (1 : 50; [46]). Desmin (PDE; Euro-Diagnostica, The Netherlands) and mouse monoclonal anti-desmin (D33; DakoCytomation), keratin (LE41; mouse monoclonal) and GFAP (polyclonal 3270 and monoclonal GA5) were as described [58]. After washing with PBS/BSA/azide, the primary antibodies were detected using FITC (1 : 100; Sigma, UK), Texas-Red (1 : 200; Jackson ImmunoResearch Laboratories, UK) or Alexa 594 (1 : 500; Molecular Probe, UK) conjugated secondary antibodies.

(j) Preparation of cell lysates and immunoblotting analysis

Cells plated at a density of 1×10^6 cells per 100 mm Petri dish were transfected with expression vectors as indicated. After 48 h, cell lysates were prepared [26] and analysed by immunoblotting followed by enhanced chemiluminescence using a luminescent image analyser (LAS-1000plus; FujiFilm, Japan).

(k) Live cell imaging and movie preparation

For live cell imaging, cells transfected with pcDNA3.1-IRES-DsRED2-Mito vectors were cultured in standard culture medium containing 10 mM HEPES, pH 7.0. in glass-bottomed culture dishes (Iwaki) and maintained at 37°C in a humidified chamber. At 24 h after transfection, time-lapse images were acquired in an Axiovert 200 inverted microscope equipped

with a charge-coupled device camera (AxioCam; Carl Zeiss, Jena, Germany) using the AxioVision (Carl Zeiss, Jena, Germany) software. Real-time images were acquired every 10 min for 12 h using a standard Rhodamine filter set (excitation at 550 nm and emission at 590–650 nm) at 40× magnification. Short exposure time and a neutral density filter were used during image acquisition to minimize photobleaching and phototoxicity. Digitized images were imported into QUICKTIME Software (QUICKTIME v. 5.0; Apple, Cupertino, CA, USA) and converted into movies.

3. Results and discussion

(a) Determination of oligomeric sizes of wild-type and mutant sHSPs

Previous studies showed that the R120G mutation in CRYAB altered its secondary, tertiary and quaternary structure [25]. To extend these findings, the corresponding mutations in human HSP27 (R140G) and in *C. elegans* HSP16.2 (R95G) were generated by site-directed mutagenesis and compared with R120G CRYAB by SEC. WT CRYAB (figure 1a) and HSP27 (figure 1b) eluted at positions corresponding to average molecular sizes of approximately 520 and 560 kDa, respectively (table 1), which is consistent with previous published results [25,61]. The arginine mutation significantly altered the molecular masses of R120G CRYAB and R140G HSP27 (figure 1a and table 1), but with opposite consequences. R140G HSP27 formed a polydisperse population of protein oligomers ranging in size from over 600 kDa to approximately 50 kDa (figure 1b), which was smaller than the WT HSP27. R120G CRYAB on the other hand was larger (684 kDa) than the WT CRYAB and also appeared no more polydisperse than the WT. There was no major effect

Table 1. SEC analysis of sHSP oligomers.

molecular masses[a] of WT sHSPs and their mutants	
WT/mutant sHSP	apparent Mr(kDa)
WT HSP16.2	572 $\pm$ 72
R95G HSP16.2	584 $\pm$ 80
WT αB-crystallin	520 $\pm$ 84
R120G αB-crystallin	684 $\pm$ 78
WT HSP27	560 $\pm$ 74
R140G HSP27	150 $\pm$ 242

[a]Molecular masses (M) were determined from a plot of logM versus V_e/V_o of molecular mass standards.

upon the assembly of the oligomeric complexes of HSP16.2 when the equivalent arginine residue (R95) was mutated (figure 1c). The R95G mutant eluted with almost the same elution volume as that of WT HSP16.2 with an apparent molecular mass of approximately 580 kDa (figure 1c and table 1). The three mutants therefore cover the range of potential consequences for the quaternary structure of sHSPs after the introduction of a glycine residue instead of arginine at this conserved site, by either reducing or increasing the oligomer size or producing no apparent change.

(b) Effect of the sHSP arginine mutations upon their co-sedimentation with intermediate filaments and preventing filament–filament associations

Several *in vitro* assays have been developed to study the effect of the R120G mutation on the interaction of CRYAB with intermediate filaments. These include the ability of sHSPs to co-sediment with intermediate filaments and to prevent filament–filament interactions as detected by falling ball viscometry [51]. Vimentin and GFAP, but not desmin, have been tested in the falling ball assay. Desmin is the physiological target for CRYAB in muscle as revealed by the phenocopying of the disease, desmin-related myopathy, by both desmin and CRYAB mutations [1].

In vitro intermediate filament co-sedimentation assays were conducted using optimized pH and salt conditions [26]. Under these conditions, desmin was assembled and sedimented efficiently as shown by the proportion of the protein partitioning into the pellet fraction in the control (figure 2a). Both the WT and R120G CRYAB (figure 2a) bind to desmin filaments in a temperature-dependent manner. The increased co-sedimentation of R120G CRYAB with desmin filaments compared with WT protein (figure 2a) was apparent at all three temperatures. Even at 37°C, almost all of the R120G CRYAB was found to bind to pelletable desmin filaments, whereas the binding of WT protein to desmin was incomplete with a small proportion still remaining in the supernatant fractions (figure 2a). For the experiments presented in figure 2a, a 1:1 molar ratio of desmin:CRYAB was used, although similar results were obtained with decreasing molar ratios at 1:0.5, 1:0.2 and 1:0.1 (data not shown). The binding of HSP27 to desmin filaments (figure 2b) was apparently less efficient than HSP16.2 (figure 2c)

and CRYAB (figure 2a). When included at a 1:1 molar ratio, the WT HSP27 showed limited binding to desmin filaments with co-sedimentation being greatest at 44°C (figure 2b). The co-sedimentation of R140G HSP27 to desmin filaments can be detected at 22°C and this remained unaltered at elevated temperatures (figure 2b). The R140G HSP27 appeared to co-sediment more efficiently with desmin filaments than WT HSP27.

In contrast to both CRYAB and HSP27, WT HSP16.2 only partially co-sedimented with desmin filaments (figure 2c). We selected this particular sHSP as a representative of those expressed in the animal *C. elegans*. It is a stress-induced sHSP in this animal and multimerization is important to its function [62]. There are also cytoplasmic intermediate filaments in *C. elegans*, albeit quite different in primary sequence to mammalian desmin [63]. The co-sedimentation of HSP16.2 appeared to be independent of temperature, as the WT protein was similarly distributed between supernatant (S) and pellet (P) fractions irrespective of temperature. Similar results were obtained for R95G HSP16.2 (figure 2c). Therefore, for this mutant, minimal effect upon the quaternary structure of the protein coincided with little change in the co-sedimentation properties with desmin filaments.

Of the three sHSPs and their respective arginine mutants, it was the R120G CRYAB that was most affected. We therefore considered whether this would alter the co-sedimentation of CRYAB with *in vitro* assembled keratin filaments (figure 2d). Filaments of keratins 7 and 18 also co-sedimented with WT CRYAB and co-sedimentation was significantly increased by the R120G CRYAB mutation, mimicking the results obtained with desmin. These data suggest that the increased co-sedimentation of CRYAB R120G is not necessarily restricted to desmin, but includes other type III intermediate filaments, in particular vimentin and GFAP, and also keratins (this study).

To assess the possible function of these various sHSPs and their arginine mutants, an assay to measure the effect of sHSPs upon filament–filament interactions was developed [51]. This assay is based upon falling ball viscometry, which provides a measure of sHSP-desmin interactions at equilibrium. Desmin filaments form a gel capable of supporting the metal ball used in the assay. The effect of the arginine mutations upon the chaperone activity of sHSP was tested. Previous studies showed that the addition of sHSPs, including CRYAB and HSP25, to assembling intermediate filament solutions prevented gel formation and so permitted the ball to sink to the bottom of the tube, even though filament assembly was not inhibited [51]. As expected, after the assembly of desmin, a gel formed preventing the ball from falling to the bottom of the tube. The presence of WT human CRYAB, *C. elegans* HSP16.2 and HSP27 with desmin allowed the ball bearing to sink to the bottom of the capillary (table 2). These WT sHSPs are apparently very effective at preventing gel formation over a 10-fold concentration range (table 2). The R95G mutation did not abolish the activity of HSP16.2 in this assay. In contrast, the mutant R120G CRYAB appeared completely ineffective at inhibiting gel formation, the ball remaining on top of the assembled desmin sample in the capillary. HSP27 R140G was equally effective as the WT protein at 1:1 ratios, but was ineffective at the 0.2:1 ratio, in contrast to the WT HSP27 (table 2).

This assay provides a rapid way to assess the potential activity of different intermediate filament and sHSP combinations. In table 3, we provide additional evidence that
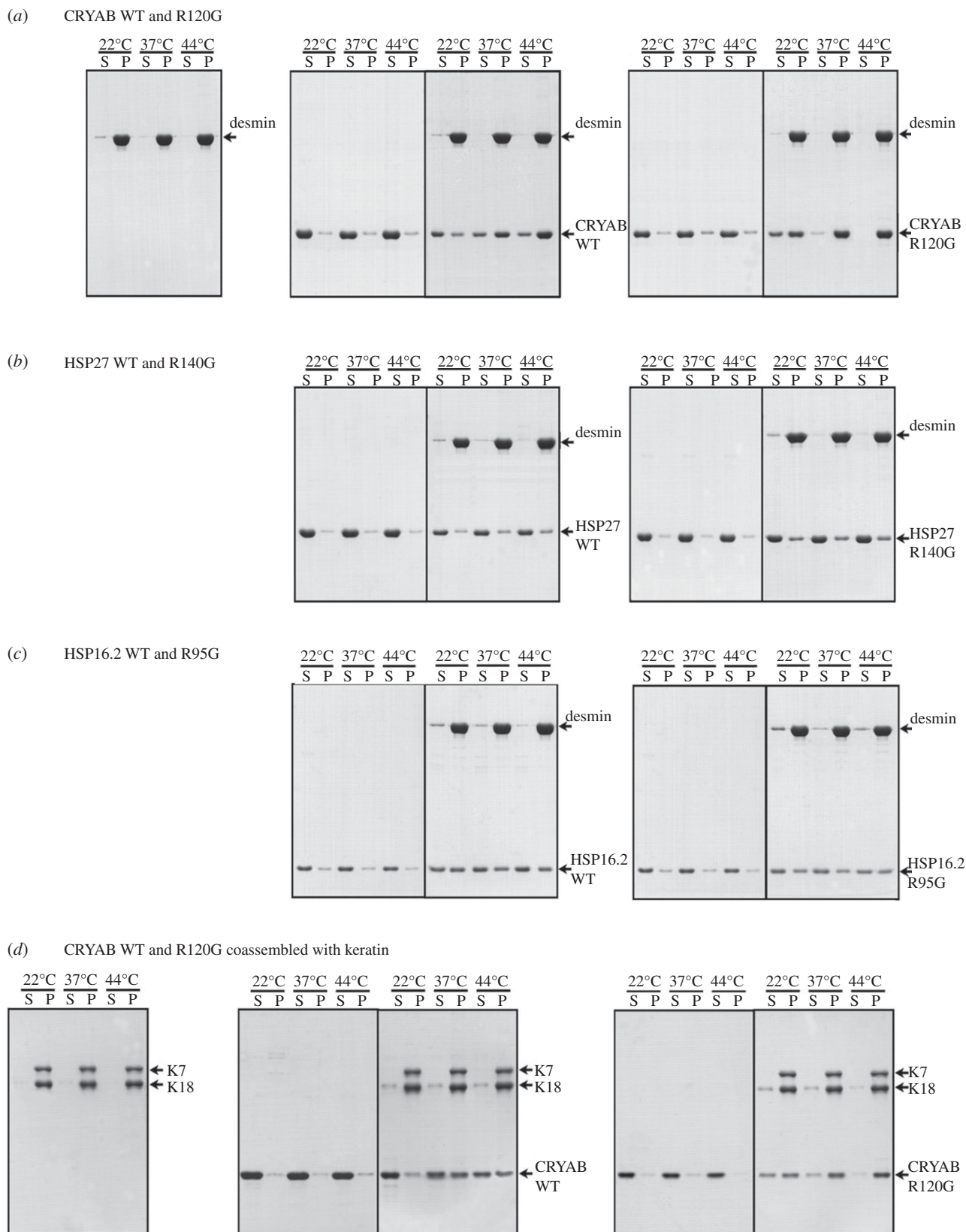
Figure 2. Co-sedimentation of WT and arginine mutant sHSPs to desmin filaments *in vitro*. In this binding assay, the assembly was conducted at temperatures indicated above the relevant gel tracks (*a–c*). The pellet (P) and supernatant (S) fractions from the co-sedimentation assays were analysed by SDS-PAGE and visualized by Coomassie Blue staining. The positions of desmin (*a–c*), keratin (*d*), WT and arginine mutants of CRYAB (*a,d*) HSP27 (*b*) and Hsp16.2 (*c*) are indicated (arrows).

sHSPs from evolutionary-unrelated organisms appear to have an innate ability to affect desmin gel formation in this falling bead assay. As an extreme test of this concept, the chloroplast-specific sHSP, HSP21 [64], was found to be able to prevent desmin gel formation. It was therefore surprising that another potential desmin-interacting mammalian sHSP,

HSP20, is not equivalent to CRYAB in this assay. HSP20 is involved in cardioprotection and can also coassemble with both HSP27 and CRYAB [65,66]. These data suggest that while sHSPs from distant organisms can affect gel formation, the different mammalian sHSPs do not possess completely equivalent properties.

Table 2. Summary of the data collected for the effect of sHSPs and their arginine mutants on the gel formation by desmin filaments as monitored by the falling ball assay. Desmin can form a protein gel capable of supporting a small stainless steel ball. Addition of WT sHSPs in a range of molar ratios from 1:1 to 0.1:1 to desmin allow filament assembly but then prevent gel formation. In this case, the ball will descend easily into the bottom of the capillary tube. A similar result was obtained for R95G HSP16.2. The R120G CRYAB abrogated this activity of αB-crystallin even over a 10-fold concentration range. The inhibitory effect of R140G HSP27 on gel formation is compromised, but not completely abolished, as this mutant can still prevent gel formation when added at a 1:1 molar ratio.

WT and mutant sHSPs added to assay	desmin gel formation as indicated by the ball position		
sHSP : desmin (molar ratio)	1 : 1	0.2 : 1	0.1 : 1
WT CRYAB	bottom	bottom	bottom
R120G CRYAB	top	top	top
WT HSP27	bottom	bottom	bottom
R140G HSP27	bottom	top	top
WT HSP16.2	bottom	bottom	bottom
R95G HSP16.2	bottom	bottom	bottom

(c) Measuring CRYAB interactions with type III intermediate filament proteins using non-equilibrium and equilibrium methods

SPR provides an equilibrium method to assess the relative binding of WT and R120G CRYAB to desmin, GFAP and vimentin (figure 3a). It can be seen that both WT and R120G CRYAB had a greater capacity for binding desmin than the other type III intermediate filament proteins, vimentin or GFAP. Moreover, there was a significant increase in the binding of R120G CRYAB to all three type III intermediate filament proteins. These data support the interpretation that there is selectivity in CRYAB binding to type III intermediate filament proteins and that the R120G mutation increases the binding of CRYAB to intermediate filaments supporting the *in vitro* co-sedimentation data and electron microscopy data [25,26]. More detailed interpretation of these data is complicated by the uncertainty over which intermediate filament assembly form is bound to the chip surface given that, at 20 μg ml^{-1}, both desmin [67] and vimentin [68,69] have the potential to form filaments while this is likely not the case for GFAP, which has a critical concentration of 80 μg ml^{-1} [70]. Purging the chip with 6 M guanidine hydrochloride should ensure that only intermediate filament monomers are bound to the chip surface. On-chip association of subunits, however, is a possibility once binding-buffer conditions are restored. Furthermore, the inherent polydispersity of CRYAB [71] further complicates the interpretation as it is not known whether there is any selectivity by specific CRYAB oligomers for intermediate filaments. SPR has been used to study CRYAB subunit dynamics [72] and to assess the relative affinity of different client proteins [73]. These data confirm the preference of CRYAB for desmin and, from

Table 3. Effect of WT and mutant sHSPs on the gel formation by desmin filaments as monitored by the falling ball assay. Inter-filament interactions between assembled desmin filaments lead to the formation of a protein gel that is capable of supporting a small stainless steel ball. Addition of sHSPs in a molar ratio of 1:1 to desmin prevented this gel formation, thus allowing the ball to drop to the bottom of the capillary tube. Carbonic anhydrase was used as a control in these experiments.

sHSPs added to desmin solution	ball position
no addition	top
carbonic anhydrase	top
CRYAB (HSPB5)	bottom
HSP21 (*Arabidopsis thaliana*)	bottom
HSP20 (HSPB6)	top

the dissociation kinetics, it is clear that once bound, CRYAB dissociates slowly from all three type III intermediate filament proteins. This would fit the conclusion that there is a high affinity binding site for CRYAB clients [74] and that topologically distinct sites are present on CRYAB [75] for these different clients as born out by peptide array studies [76]. With respect to a protein polymer such as an intermediate filament, the rules for client selection by sHSPs may not parallel those established for monomeric, destabilized clients such as T4 lysozyme [75,77]. Indeed there is no evidence currently to suggest that intermediate filament proteins naturally adopt unfolded conformations within the filament, although this can be induced by mechanical stretching [78]. There is, however, evidence to suggest that filaments exhibit different subunit geometries that can be differentially detected by antibodies [79,80] and could be induced by post-translational modifications [19,81–87]. The presence of disease-causing mutants or GFP-tagged intermediate proteins is sufficient to increase the binding of CRYAB to the filaments [58,88], which we interpret as evidence of altered subunit geometries inducing sHSP association with intermediate filaments.

Using Ostwald viscometry, the assembly of GFAP in the presence of WT and R120G CRYAB was analysed (figure 3b). Addition of CRYAB reduced the overall viscosity of the solution, but the presence of the R120G CRYAB induced a catastrophic loss of viscosity after approximately 25 min when aggregates were visible in the solution consistent with the falling ball assay. We confirmed the presence of highly bundled filaments by electron microscopy (see the electronic supplementary material, figure S1). These data indicate the ability of WT CRYAB to reduce the apparent viscosity of a solution of GFAP filaments. In contrast, the presence of R120G CRYAB promotes interactions between GFAP filaments, which induces clumping and their eventual aggregation, which has the effect of significantly reducing solution viscosity, but by a completely different mechanism and with greater impact than the viscosity reduction induced by WT CRYAB. The effect of the R120G mutation is to drive the aggregation of the GFAP filaments.

A disadvantage of the Ostwald viscometer is that flow-induced filament orientation occurs during the measurements, which may lead to shear-thinning. For this reason, we turned to a passive rheology approach using optically trapped beads (figure 3c). As intermediate filaments are semi-flexible polymers that show both elastic and viscous
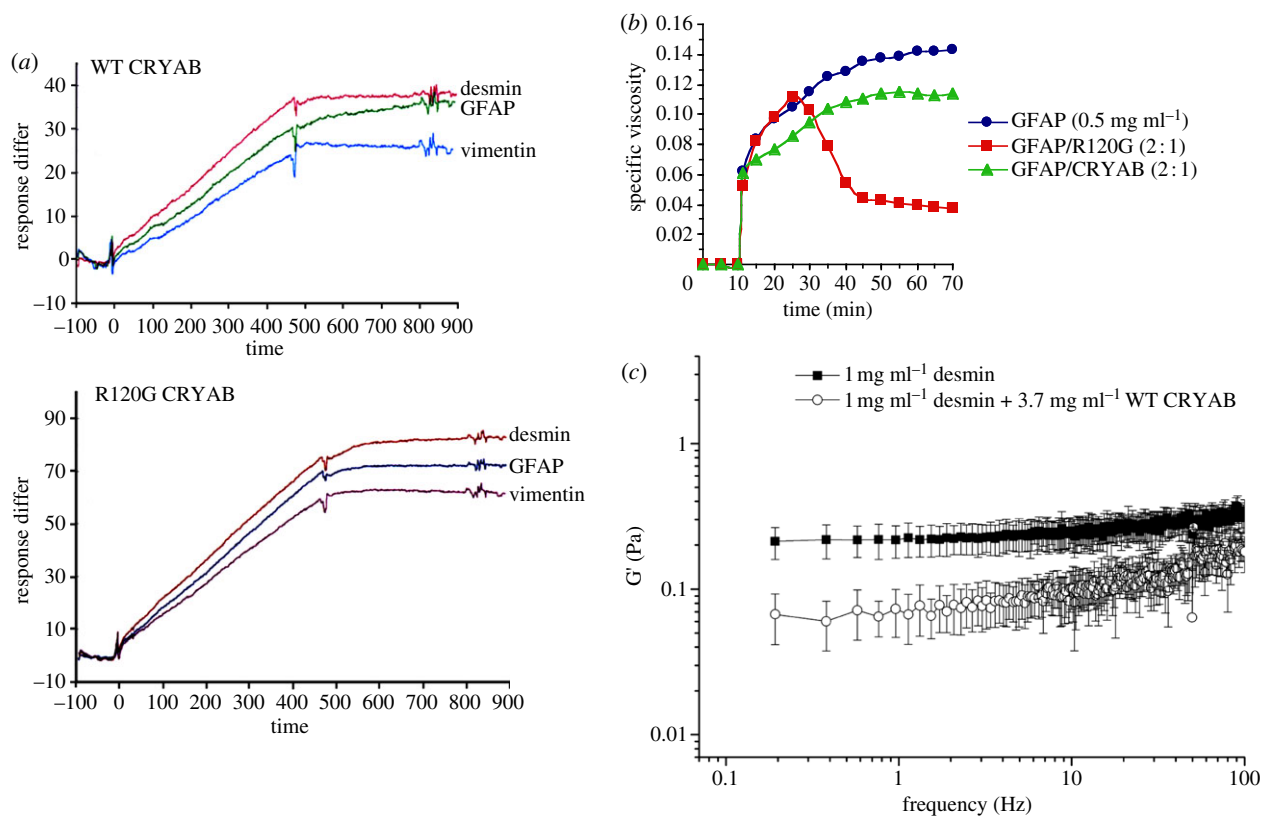
Figure 3. Equilibrium methods of detecting the interaction of CRYAB with intermediate filaments. (a) Binding kinetics of WT and R120G CRYAB to different intermediate filament (IF) proteins as measured by SPR. Desmin, GFAP and vimentin were immobilized to the dextran matrix of a CM5 sensor chip. Binding of 20 g ml WT (a) or R120G (b) CRYAB to immobilized IF proteins were monitored at 37°C for 7.5 min, followed by washing for 7.5 min. Measurements were performed at a flow rate of 5 l min^{-1} using a Biacore 3000 Biosensor. Resonance measured during 900 s of exposure is plotted on the ordinate in arbitrary units. (b) Viscometric analyses of GFAP assembly in the absence or presence of CRYAB. GFAP (0.5 mg ml^{-1}) was assembled either alone or coassembled with either WT or R120G CRYAB in a molar ratio of 1 : 2 at 37°C. Assembly was initiated at the 10 min time-point by addition of a 20-fold concentrated assembly buffer. Specific viscosity was measured 1 min after assembly and then at 5 min intervals for 60 min. The profile obtained for GFAP reflects the normal increase of specific viscosity after initiation of filament assembly. In the presence of WT CRYAB, GFAP exhibited a slightly decreased specific viscosity over a period of 40–45 min before reaching a plateau. In contrast, for GFAP assembled in the presence of R120G CRYAB, the specific viscosity increased normally only during the first 25 min. Afterward it decreased dramatically, indicative of GFAP filament aggregation. (c) Passive rheology measurements by one-particle microrheology. WT desmin was assembled alone or with a 1 : 10 molar ratio of WT desmin: WT CRYAB. The position fluctuations of beads immersed in the network were measured by trapping beads with a weak 808 nm laser and measuring scattered light on a QPD. The elastic modulus was corrected for the presence of the optical trap. Average G' values (Pa) ±1 s.d. from five independently trapped beads for WT desmin and from 10 independently trapped beads for WT desmin with WT CRYAB are plotted against frequency (Hz). Desmin assembled alone has a higher stiffness compared with when WT CRYAB is present. This difference is statistically significant with $p \leq 0.01$, using a type 2, one-tailed Student's t-test. (Online version in colour.)

properties, bulk rheology has been used to assess the mechanical properties of desmin networks in terms of their flexibility and persistence lengths [89]. We find that CRYAB slightly reduces the elastic modulus of the desmin filament networks as measured by one-particle passive microrheology (figure 3c). This confirms the interaction of CRYAB with intermediate filaments, eliciting a measurable change in the biomechanical properties of the filament solution. The divalent cation-mediated interaction of C-terminal sequences of the type III intermediate filament proteins could partly explain the filament solution properties [90] and parallels the similar role for the C-terminal extensions in neurofilaments [91]. The precise details of how CRYAB might prevent the filament–filament interactions as measured by the falling ball (table 2; [51]), low-speed sedimentation [26,52] and viscosity assays (figure 3b) is not yet determined and neither is the question of how this relates to the observed reduction in the stiffness of the desmin filament network. Nevertheless, for other poly-electrolyte systems such as

actin [92] and neurofilaments [91,93], the cations and pH in solution and the amino acid sequence exposed at the filament surface are known to be key factors in driving gel formation, sHSP association and thus sample stiffness.

(d) Temperature and pH dependency of the interaction of CRYAB with desmin, GFAP and vimentin intermediate filaments

Desmin, GFAP and vimentin were assembled *in vitro* at three different pH values and temperatures to see how these variables influenced CRYAB association. Previous studies with recombinant purified human intermediate filament proteins have looked at temperature effects (e.g. [67]), but not pH effects, although the CRYAB association with a mixture of desmin and actin at different pHs was investigated previously [94]. Intermediate filaments were formed at all pHs and temperatures analysed (figure 4e,f; data not shown for GFAP and
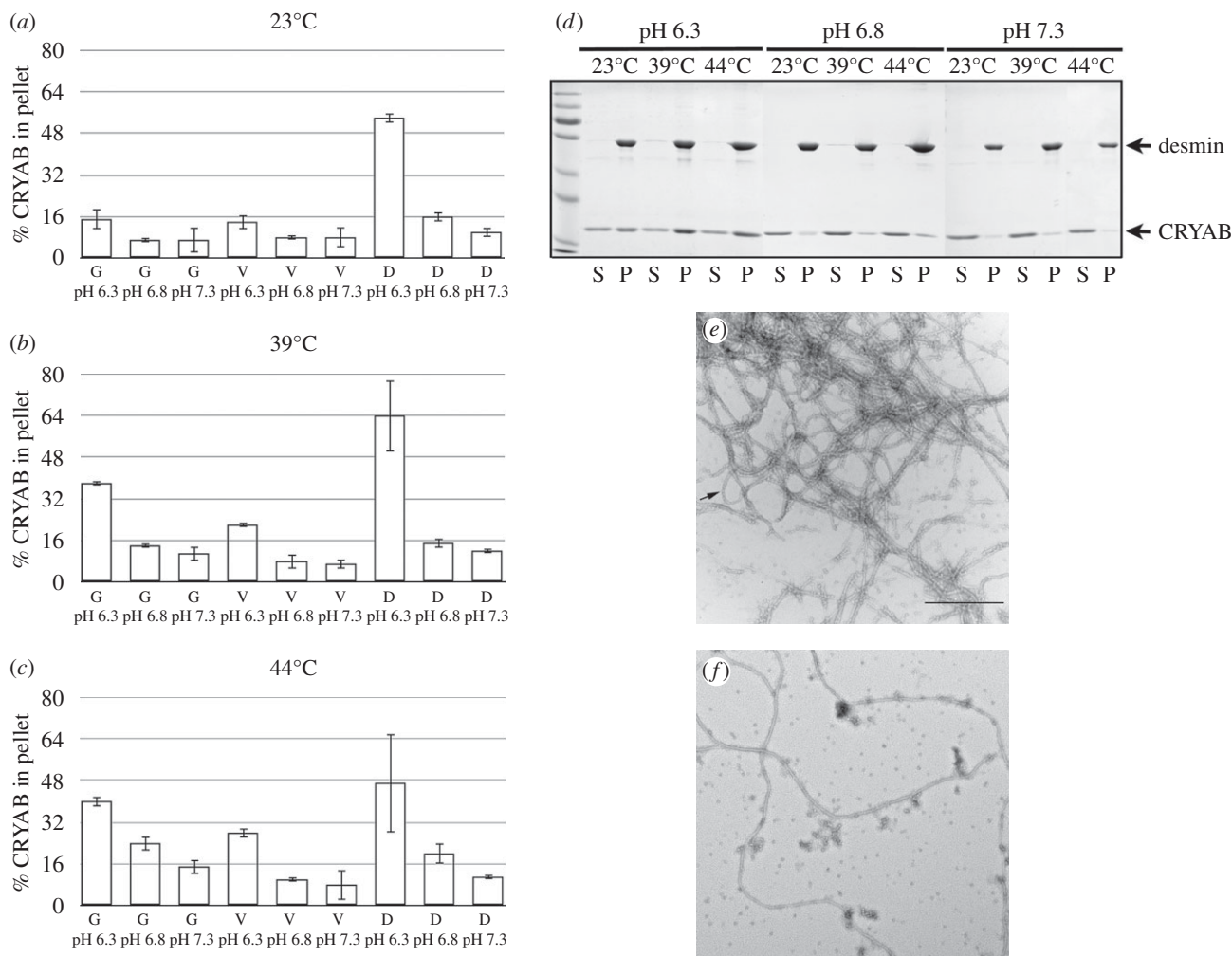
Figure 4. CRYAB interaction with desmin is divalent cation-, pH- and temperature-dependent. Binding of CRYAB to desmin, GFAP and vimentin filaments was assessed by high-speed co-sedimentation assay (a–d). The quantified results are presented as the mean $\pm$ s.d. of the percentage of CRYAB that had co-sedimented with WT desmin, GFAP and vimentin at 23°C, 39°C and 44°C (a–c, respectively). Note, most binding occurs at pH 6.3 and at 39°C and 44°C with a preference for desmin over vimentin and GFAP. A representative gel image used for the quantification of binding to desmin is shown (d). Three independent experiments were used for the quantifications. (e,f) WT desmin formed filaments of a few micrometres in length and had a much higher density of CRYAB particles (arrow) surrounding the filaments at pH 6.3 (e) compared with pH 7.3 (f). Images are taken at the same magnification. Scale bar, 500 nm. G, GFAP; V, vimentin; D, desmin; S, supernatant; P, pellet.

vimentin). Desmin filaments were coated with CRYAB particles at pH 6.3 and at 23°C (figure 4e,f). High-speed co-sedimentation analyses showed that at pH 6.3 and over the temperature range from 39°C to 44°C, more than 35 per cent of the total CRYAB was associated with the desmin and GFAP filaments. In line with the SPR data, CRYAB binding followed the same trend, with desmin binding the most and vimentin the least (figure 4a–c) at the temperatures and pHs investigated. Lower binding was observed at pH 7.3 and 6.8 (figure 4a–c) indicating that there was a pH dependency in CRYAB binding to desmin, GFAP and vimentin. We also investigated the pH effects on the binding of CRYAB to pre-formed GFAP filaments by co-sedimentation and observed a similar trend of increased binding at pH 6.3 that was also temperature-dependent (data not shown). Similar studies were not possible for desmin, as in the absence of CRYAB desmin filaments were attracted to the plastic surfaces of tips and tubes (data not shown).

Ischaemia results in a pH decline in muscle tissue [95] and the translocation to the Z- and I-bands of resident sHSPs [96,97], which is the location of the desmin intermediate filaments. Therefore, the data we have presented evidence the importance

of pH changes to the interaction of CRYAB with desmin. The structure of CRYAB would be expected to change in acidosis, resulting in a dimer-monomer transition of the α-crystallin domain [98,99] as well as its activation [100]. The R120G mutation in CRYAB, in contrast, stabilized its dimers at low pH [101], the result of removal of a positive charge from within the dimer interface which contains histidines sensitive to physiological pH changes [44,98]. Therefore, it appears that acidic pH can induce the release of monomeric WT CRYAB, but not the R120G mutant. This perhaps leads to extended interactions with desmin filaments, compared with WT CRYAB, at physiological pH values as evidenced by the studies here and those previously published [25,26,102].

(e) Transient transfection studies

In order to determine the effect of these arginine mutations upon the potential *in vivo* activity of the respective sHSPs, transient transfection assays were performed. Desmin filaments form characteristic aggregates as part of the histopathology in the cardiomyopathies so far described with the R120G CRYAB mutation. As a mimic of this situation, desmin was
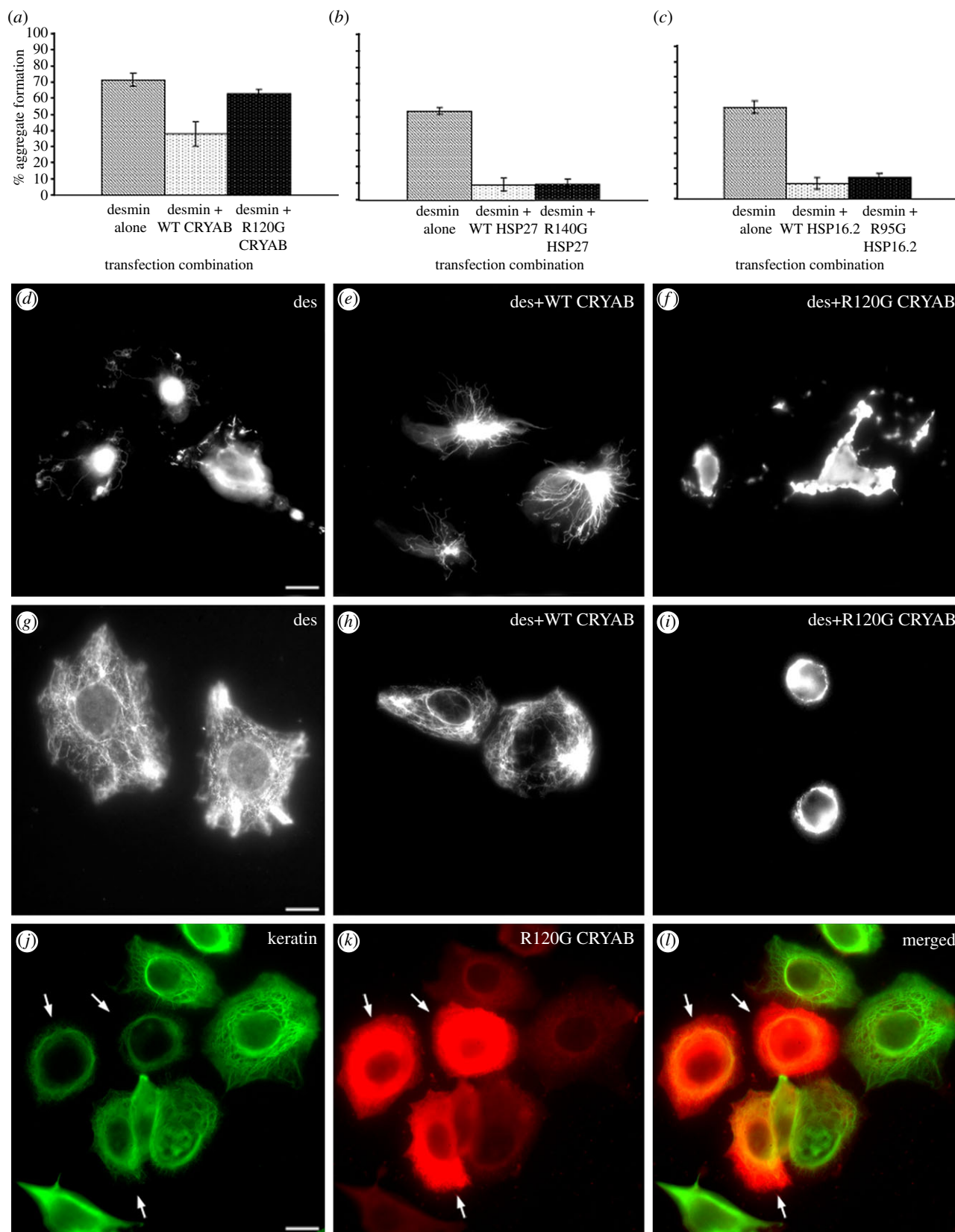
Figure 5. Expression of R120G CRYAB induces the aggregation of intermediate filaments. (*a–c*) The immortalized human lens epithelial cell line H36CE2 was transiently transfected with combinations of desmin with either WT CRYAB or R120G CRYAB (*a*), with desmin and either WT HSP27 or R140G HSP27 (*b*) and with desmin and either WT HSP16.2 or R95G HSP16.2 (*c*). The number of desmin aggregate-containing cells were then counted and the mean ± s.d. calculated and plotted as bar charts. R120G CRYAB was the only mutant sHSP that significantly increased the number of desmin aggregates in the transiently transfected cells. Representatives of transfected cells are not shown. (*d–f*). (*d*) SW13 Vim⁻ cells were transiently co-transfected with desmin alone, (*e*) desmin and WT CRYAB and (*f*) desmin and R120G CRYAB. Note the aggregates in those cells co-transfected with desmin and R120G CRYAB. (*g–i*) The effect of the transient transfection of WT CRYAB and R120G CRYAB upon the endogenous keratin networks in MCF7 cells. (*g*) MCF7 cells were transiently co-transfected with desmin alone, (*h*) desmin and WT CRYAB and (*i*) desmin and R120G CRYAB. (*j–k*) Transient transfection of MCF7 cells with R120G CRYAB. (*j*) Cells were then probed with both keratin and (*k*) CRYAB antibodies. Note that in the R120G CRYAB transfected cells the endogenous keratin networks have collapsed around the nucleus, indicating the ability of CRYAB R120G to act in a dominant negative fashion to aggregate keratin filaments. Scale bar, 10 μm.
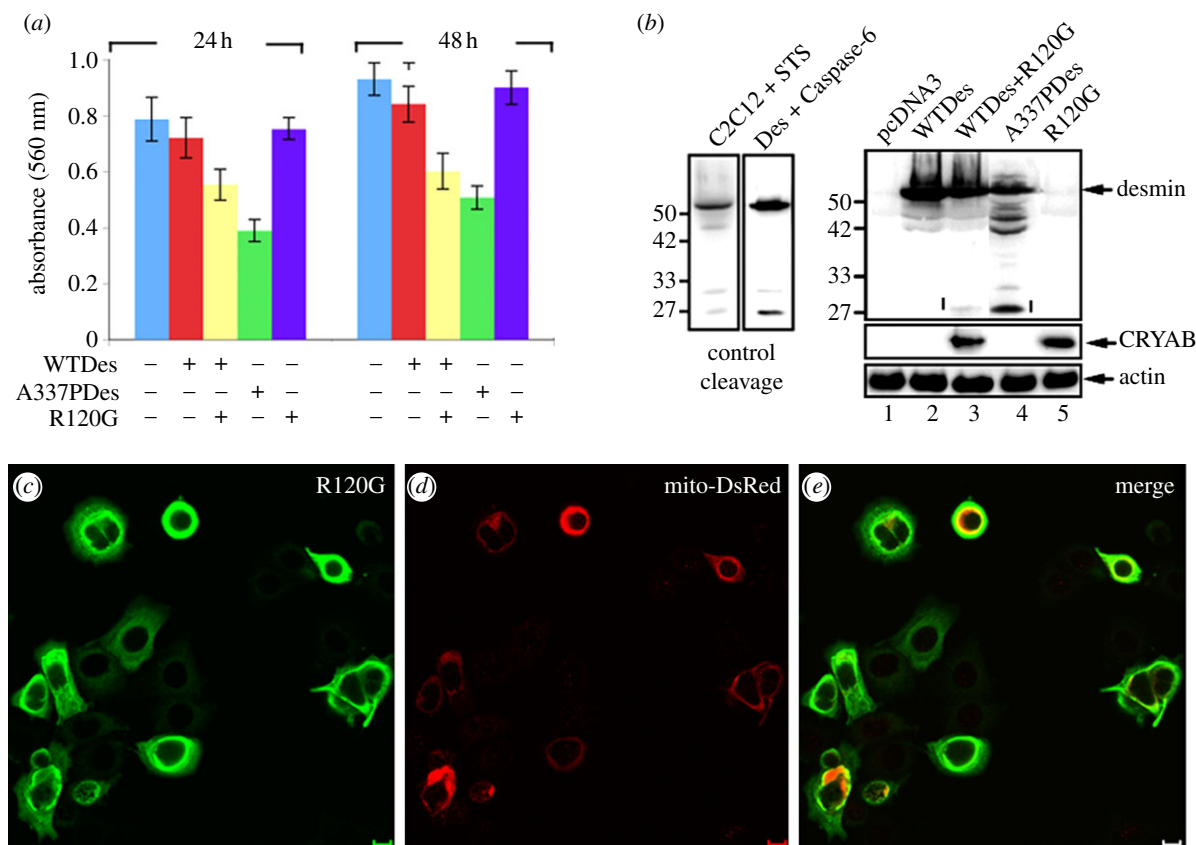
Figure 6. Expression of mutant desmins reduces viability of MCF7 cells. (*a*) Cell viability was measured in MCF7 cells transiently transfected with WT desmin, A337P desmin, R120G CRYAB alone or co-transfected with WT desmin and R120G CRYAB at a 1 : 1 molar ratio. Cells transfected with empty pcDNA3.1 vector were used as a control. The viability of transfected MCF7 cells was determined at 24 and 48 h using the MTS-based cell viability assay. Data shown are the mean $\pm$ s.e. from three independent experiments. Statistical significance was analysed by one-way ANOVA and the level of significance was set at $p \leq 0.05$. (*b*) Desmin fragmentation by caspases. Two desmin fragments (arrowheads) were generated in C2C12 cells induced to undergo apoptosis by treatment with 1 μM staurosporine (C2C12 + STS) and *in vitro* by cleavage of purified desmin with active caspase 6 (Des + Caspase 6). One of the proteolytic fragments was faintly observed in cells co-transfected with WT desmin and R120G αB-crystallin (lane 3). Levels of protein expressed in transfected MCF7 cells were determined at 48 h after transfection. Immunoblotting of total cell lysates and probing with antibodies to desmin, CRYAB and finally actin, as a loading control. (*c*–*e*) To determine the effect of expressing R120G CRYAB (green channel) upon the distribution of mitochondria, MCF7 cells were transiently transfected with an IRES-containing bicistronic vector that allows simultaneously expression of both mitochondrially targeted red fluorescent protein (*c*; red channel) and R120G CRYAB (*d*; green channel). Note the collapse of the mitochondria into perinuclear locations in those cells (*e*; merged red and green channels) expressing R120G CRYAB.

co-transfected with either the WT or mutant sHSP and the formation of desmin aggregates compared with that of desmin alone. The human cell line H36CE2 was chosen because it is a human cell line that does not express desmin, but does express vimentin. Lens epithelial cells can express desmin as part of their response to posterior capsule opacification [103]. The results were recorded as the percentage of cells with desmin-positive aggregates.

The transfection of desmin into H36CE2 cells leads to the formation of desmin-positive aggregates in the cytoplasm of a high proportion of the cells. Co-transfection with CRYAB significantly reduced the incidence of aggregate-positive cells, but when the R120G CRYAB was co-transfected with desmin, this positive effect was lost and desmin aggregates were once again apparent (figure 5*a*). In contrast, the co-transfection of either HSP27 or R140G HSP27 (figure 5*b*) or HSP16.2 or R95G HSP16.2 (figure 5*c*) all significantly reduced desmin aggregate formation in transfected H36CE2 cells.

We selected two other cell lines to confirm the tendency of R120G CRYAB to induce the aggregation of desmin filaments in transiently transfected cells. In SW13/Cl2 Vim$^-$ cells, an adenocarcinoma cell line that lacks cytoplasmic intermediate filaments, the transiently transfected desmin also failed to form effective networks of desmin filament (figure 5*d*). Only

when co-transfected with WT CRYAB (figure 5*e*) were desmin filament networks observed. As with H36CE2 cells, co-transfection of desmin with R120G CRYAB induced desmin filament aggregation (figure 5*f*). These aggregates costained with CRYAB antibodies (data not shown). A similar experimental series is also shown for MCF7 cells, which have an endogenous cytoplasmic keratin network, showing similar results for co-transfection of WT and R120 CRYAB, albeit in these cells desmin alone was capable of forming a filament network (figure 5*g*–*i*). The co-transfection of R120G CRYAB with desmin caused the perinuclear collapse of the desmin filaments (figure 5*i*). Interestingly, the transient transfection of R120G CRYAB into MCF7 cells was also capable of causing the collapse of the endogenous keratin network of filaments (figure 5*j,k*), but there was no loss in cell viability.

In the course of these experiments involving MCF7 cells, we noticed low transfection rates for the desmin when co-transfected with R120G CRYAB. We therefore monitored cell viability after transfection. We included a series of controls including the DRM-causing desmin mutant A337P. The results are presented in figure 6*a*. Co-transfection of R120G CRYAB with WT desmin induced a significant reduction in cell viability. This was not observed when R120G CRYAB was transiently transfected into MCF7 cells.

Neither was the transfection of WT desmin deleterious for cell viability. Interestingly, only the DRM-causing desmin mutant A337P induced a similar reduction in cell viability. These data suggest that DRM-causing mutations in either desmin (A337P) or CRYAB (R120G) were capable of reducing cell viability, but R120G CRYAB was dependent upon the presence of desmin for this effect.

Desmin has been found to propagate the canonical apoptosis pathway, it being a substrate for caspase 6 [9] and evidenced by our control experiments using staurosporin-treated C2C12 cells and caspase 6-treated desmin (figure 6b). Similar-sized desmin proteolytic fragments were observed in samples prepared from MCF7 cells transfected with A337P desmin and for those co-transfected with the combination of WT desmin and R120G CRYAB (figure 6b). Using the modified IRES-Mito-DsRED-based pcDNA3.1 vector to identify the mitochondria of transient transfected cells, R120G CRYAB induced the collapse of mitochondria along with the perinuclear aggregation of the endogenous keratin filaments (figure 6c–e), but as evidenced by the cell viability assay (see the electronic supplementary material, figure S2) the expression of disease-causing desmin mutants induces apoptosis by the activation of caspases. The fact that R120G CRYAB induces the collapse of the endogenous keratin filaments and the mitochondria in MCF7 cells singly transfected with just R120G CRYAB is very important especially as these are phenocopied by the co-transfection of both R120G CRYAB with desmin. The important difference is that only when R120G CRYAB is co-transfected with WT desmin is there a significant decrease in cell viability, which we take as prime fascia evidence of a unique and specific interaction that sets it apart from keratins and vimentin, the intermediate filaments found in H36CE2 and MCF7 cells.

(f) CRYAB and desmin form a functional complex

The transient transfection studies suggest that desmin and CRYAB are indeed a functional complex, which can determine whether transiently transfected cells continue to proliferate or die (figure 6). Analysis of transgenic animal models have tended to overlook the functional aspect of the desmin-CRYAB interaction, focusing rather on the amyloid-forming potential of R120G CRYAB [5], or on the ability of R120G CRYAB [104,105] and desmin mutants [7] to inhibit the proteosome or affect autophagy [8,38,106]. Our studies

illustrate that, while these are important consequences, the primary lesion in the development of DRM appears to be the dominant negative effect of the desmin–CRYAB complex on cell viability. Indeed the effects of CRYAB on MCF7 cells suggests that the only muscle-specific factors required in order to precipitate the loss of viability is either a mutant desmin, or R120G CRYAB in the presence of WT desmin. This therefore suggests a very simple explanation for why R120G CRYAB induces a myopathy and not, for instance, a neuropathy, as muscle is the tissue where there is significant expression of desmin, the intermediate filament partner needed to trigger cell death and the muscle pathology [9,18]. Indeed our data also suggest that aggregation of the resident keratin intermediate filament network by R120G CRYAB and the concentration of the mitochondria in a perinuclear region are insufficient triggers for this loss in MCF7 viability. The fact that mutations in either desmin [2] or CRYAB [1] phenocopy each other further evidences this key functional link, which we suggest is fundamental to the muscle pathologies associated with the respective mutations in CRYAB and desmin. We conclude that the specific intermediate filament expression pattern must be considered as a key factor in any sHSP-based pathology and this study is further evidence of the functional importance of the sHSP-intermediate filament protein complex [41,42].

References

1. Vicart P et al. 1998 A missense mutation in the αB-crystallin chaperone gene causes a desmin-related myopathy. Nat. Genet. 20, 92–95. (doi:10.1038/1765)

2. Goldfarb LG et al. 1998 Missense mutations in desmin associated with familial cardiac and skeletal myopathy. Nat. Genet. 19, 402–403. (doi:10.1038/1300)

3. Munoz-Marmol AM et al. 1998 A dysfunctional desmin mutation in a patient with severe generalized myopathy (in process citation). Proc. Natl Acad. Sci. USA 95, 11 312–11 317. (doi:10.1073/pnas.95.19.11312)

4. Nicholl ID, Quinlan RA. 1994 Chaperone activity of a-crystallins modulates intermediate filament assembly. EMBO J. 13, 945–953.

5. Sanbe A, Osinska H, Saffitz JE, Glabe CG, Kayed R, Maloyan A, Robbins J 2004 Desmin-related cardiomyopathy in transgenic mice: a cardiac amyloidosis. Proc. Natl Acad. Sci. USA 101, 10 132–10 136. (doi:10.1073/pnas.0401900101)

6. Meehan S, Berry Y, Luisi B, Dobson CM, Carver JA, MacPhee CE. 2004 Amyloid fibril formation by lens crystallin proteins and its implications for cataract formation. J. Biol. Chem. 279, 3413–3419. (doi:10.1074/jbc.M308203200)

7. Liu J, Chen Q, Huang W, Horak KM, Zheng H, Mestril R, Wang X. 2006 Impairment of the ubiquitin-proteasome system in desminopathy mouse hearts. FASEB J. 20, 362–364.

8. Zheng Q, Su H, Ranek MJ, Wang X. 2011 Autophagy and p62 in cardiac proteinopathy. Circ. Res. 109, 296–308. (doi:10.1161/CIRCRESAHA.111.244707)

9. Chen F, Chang R, Trivedi M, Capetanaki Y, Cryns VL. 2003 Caspase proteolysis of desmin produces a dominant-negative inhibitor of intermediate filaments and promotes apoptosis. J. Biol. Chem. 278, 6848–6853. (doi:10.1074/jbc.M212021200)

10. Maloyan A, Sanbe A, Osinska H, Westfall M, Robinson D, Imahashi K, Murphy E, Robbins J. 2005 Mitochondrial dysfunction and apoptosis underlie the pathogenic process in α-B-crystallin desmin-related cardiomyopathy. Circulation 112,

3451–3461. (doi:10.1161/CIRCULATIONAHA.105.572552)

11. Hnia K, Tronchere H, Tomczak KK, Amoasii L, Schultz P, Beggs AH, Payrastre B, Mandel JL, Laporte J. 2011 Myotubularin controls desmin intermediate filament architecture and mitochondrial dynamics in human and mouse skeletal muscle. *J. Clin. Invest.* **121**, 70–85. (doi:10.1172/JCI44021)

12. Stone MR et al. 2007 Absence of keratin 19 in mice causes skeletal myopathy with mitochondrial and sarcolemmal reorganization. *J. Cell Sci.* **120**, 3999–4008. (doi:10.1242/jcs.009241)

13. Weisleder N, Taffet GE, Capetanaki Y. 2004 Bcl-2 overexpression corrects mitochondrial defects and ameliorates inherited desmin null cardiomyopathy. *Proc. Natl Acad. Sci. USA* **101**, 769–774. (doi:10.1073/pnas.0303202101)

14. Milner DJ, Mavroidis M, Weisleder N, Capetanaki Y. 2000 Desmin cytoskeleton linked to muscle mitochondrial distribution and respiratory function. *J. Cell Biol.* **150**, 1283–1298. (doi:10.1083/jcb.150.6.1283)

15. Konieczny P, Fuchs P, Reipert S, Kunz WS, Zeold A, Fischer I, Paulin D, Schroder R, Wiche G. 2008 Myofiber integrity depends on desmin network targeting to Z-disks and costameres via distinct plectin isoforms. *J. Cell Biol.* **181**, 667–681. (doi:10.1083/jcb.200711058)

16. Schroder R et al. 2003 On noxious desmin: functional effects of a novel heterozygous desmin insertion mutation on the extrasarcomeric desmin cytoskeleton and mitochondria. *Hum. Mol. Genet.* **12**, 657–669. (doi:10.1093/hmg/ddg060)

17. Kostareva A et al. 2008 Mice expressing L345P mutant desmin exhibit morphological and functional changes of skeletal and cardiac mitochondria. *J. Muscle Res. Cell Motil.* **29**, 25–36. (doi:10.1007/s10974-008-9139-8)

18. Panagopoulou P, Davos CH, Milner DJ, Varela E, Cameron J, Mann DL, Capetanaki Y. 2008 Desmin mediates TNF-α-induced aggregate formation and intercalated disk reorganization in heart failure. *J. Cell Biol.* **181**, 761–775. (doi:10.1083/jcb.200710049)

19. Diguet N et al. 2011 Muscle creatine kinase deficiency triggers both actin depolymerization and desmin disorganization by advanced glycation end products in dilated cardiomyopathy. *J. Biol. Chem.* **286**, 35 007–35 019. (doi:10.1074/jbc.M111.252395)

20. Mackiewicz U et al. 2012 Preserved cardiomyocyte function and altered desmin pattern in transgenic mouse model of dilated cardiomyopathy. *J. Mol. Cell Cardiol.* **52**, 978–987. (doi:10.1016/j.yjmcc.2012.01.008)

21. Liu J, Tang M, Mestril R, Wang X. 2006 Aberrant protein aggregation is essential for a mutant desmin to impair the proteolytic function of the ubiquitin-proteasome system in cardiomyocytes. *J. Mol. Cell Cardiol.* **40**, 451–454. (doi:10.1016/j.yjmcc.2005.12.011)

22. Wang X, Osinska H, Klevitsky R, Gerdes AM, Nieman M, Lorenz J, Hewett T, Robbins J. 2001 Expression of R120G-αB-crystallin causes aberrant desmin and

αB-crystallin aggregation and cardiomyopathy in mice. *Circ. Res.* **89**, 84–91. (doi:10.1161/hh1301.092688)

23. Andley UP, Hamilton PD, Ravi N, Weihl CC. 2011 A knock-in mouse model for the R120G mutation of αB-crystallin recapitulates human hereditary myopathy and cataracts. *PLoS ONE* **6**, e17671. (doi:10.1371/journal.pone.0017671)

24. Quinlan R, van den IJssel P. 1999 Fatal attraction: when chaperone turns harlot [news]. *Nat. Med.* **5**, 25–26. (doi:10.1038/4704)

25. Perng MD, Muchowski PJ, van den IJssel P, Wu GJS, Clark JI, Quinlan RA. 1999 The cardiomyopathy and lens cataract mutation in αB-crystallin compromises secondary, tertiary and quaternary protein structure and reduces *in vitro* chaperone activity. *J. Biol. Chem.* **274**, 33 235–33 243. (doi:10.1074/jbc.274.47.33235)

26. Perng MD, Wen SF, van den IP, Prescott AR, Quinlan RA. 2004 Desmin aggregate formation by R120G αB-crystallin is caused by altered filament interactions and is dependent upon network status in cells. *Mol. Biol. Cell* **15**, 2335–2346. (doi:10.1091/mbc.E03-12-0893)

27. Kolb SJ et al. 2010 Mutant small heat shock protein B3 causes motor neuropathy: utility of a candidate gene approach. *Neurology* **74**, 502–506. (doi:10.1212/WNL.0b013e3181cef84a)

28. Song S, Landsbury A, Dahm R, Liu Y, Zhang Q, Quinlan RA. 2009 Functions of the intermediate filament cytoskeleton in the eye lens. *J. Clin. Invest.* **119**, 1837–1848. (doi:10.1172/JCI38277)

29. Kato K, Shinohara H, Kurobe N, Goto S, Inaguma Y, Ohshima K. 1991 Immunoreactive alpha A crystallin in rat non-lenticular tissues detected with a sensitive immunoassay method. *Biochim. Biophys. Acta* **1080**, 173–180. (doi:10.1016/0167-4838(91)90146-Q)

30. Kato K, Shinohara H, Kurobe N, Inaguma Y, Shimizu K, Ohshima K. 1991 Tissue distribution and developmental profiles of immunoreactive aB crystallin in the rat non-lenticular tissues determined with a sensitive immunoassay system. *Biochim. Biophys. Acta* **1074**, 201–208. (doi:10.1016/0304-4165(91)90062-L)

31. Clemen CS et al. 2005 Hsp27–2D-gel electrophoresis is a diagnostic tool to differentiate primary desminopathies from myofibrillar myopathies. *FEBS Lett.* **579**, 3777–3782. (doi:10.1016/j.febslet.2005.05.051)

32. Paulsen G, Lauritzen F, Bayer ML, Kalhovde JM, Ugelstad I, Owe SG, Hallen J, Bergersen LH, Raastad T. 2009 Subcellular movement and expression of HSP27, αB-crystallin, and HSP70 after two bouts of eccentric exercise in humans. *J. Appl. Physiol.* **107**, 570–582. (doi:10.1152/japplphysiol.00209.2009)

33. Sanbe A et al. 2009 Protective effect of geranylgeranylacetone via enhancement of HSPB8 induction in desmin-related cardiomyopathy. *PLoS ONE* **4**, e5351. (doi:10.1371/journal.pone.0005351)

34. Almeida-Souza L et al. 2011 Small heat-shock protein HSPB1 mutants stabilize microtubules in Charcot-Marie-Tooth neuropathy. *J. Neurosci.* **31**,

15 320–15 328. (doi:10.1523/JNEUROSCI.3266-11.2011)

35. d'Ydewalle C et al. 2011 HDAC6 inhibitors reverse axonal loss in a mouse model of mutant HSPB1-induced Charcot-Marie-Tooth disease. *Nat. Med.* **17**, 968–974. (doi:10.1038/nm.2396)

36. Hishiya A, Salman MN, Carra S, Kampinga HH, Takayama S. 2011 BAG3 directly interacts with mutated αB-crystallin to suppress its aggregation and toxicity. *PLoS ONE* **6**, e16828. (doi:10.1371/journal.pone.0016828)

37. Irobi J et al. 2010 Mutant HSPB8 causes motor neuron-specific neurite degeneration. *Hum. Mol. Genet.* **19**, 3254–3265. (doi:10.1093/hmg/ddq234)

38. Maloyan A, Sayegh J, Osinska H, Chua BH, Robbins J. 2010 Manipulation of death pathways in desmin-related cardiomyopathy. *Circ. Res.* **106**, 1524–1532. (doi:10.1161/CIRCRESAHA.109.212639)

39. Sun X et al. 2010 Abnormal interaction of motor neuropathy-associated mutant HspB8 (Hsp22) forms with the RNA helicase Ddx20 (gemin3). *Cell Stress Chaperones* **15**, 567–582. (doi:10.1007/s12192-010-0169-y)

40. Zhai J, Lin H, Julien JP, Schlaepfer WW. 2007 Disruption of neurofilament network with aggregation of light neurofilament protein: a common pathway leading to motor neuron degeneration due to Charcot-Marie-Tooth disease-linked mutations in NFL and HSPB1. *Hum. Mol. Genet.* **16**, 3103–3116. (doi:10.1093/hmg/ddm272)

41. Quinlan R. 2002 Cytoskeletal competence requires protein chaperones. *Prog. Mol. Subcell. Biol.* **28**, 219–233. (doi:10.1007/978-3-642-56348-5_12)

42. Quinlan RA. 2010 Functional symbiosis between the intermediate filament cytoskeleton and small heat shock proteins. In *Small stress proteins and human disease* (ed. SSaA-P Arrigo). Hauppauge, NY: Nova Science.

43. Eriksson JE, Dechat T, Grin B, Helfand B, Mendez M, Pallari HM, Goldman RD. 2009 Introducing intermediate filaments: from discovery to disease. *J. Clin. Invest.* **119**, 1763–1771. (doi:10.1172/JCI38339)

44. Clark AR, Naylor CE, Bagneris C, Keep NH, Slingsby C. 2011 Crystal structure of R120G disease mutant of human αB-crystallin domain dimer shows closure of a groove. *J. Mol. Biol.* **408**, 118–134. (doi:10.1016/j.jmb.2011.02.020)

45. van den IJssel P, Wheelock R, Prescott A, Russell P, Quinlan RA. 2003 Nuclear speckle localisation of the small heat shock protein α B-crystallin and its inhibition by the R120G cardiomyopathy-linked mutation. *Exp. Cell. Res.* **287**, 249–261. (doi:10.1016/S0014-4827(03)00092-2)

46. Leroux MR, Melki R, Gordon B, Batelier G, Candido EP. 1997 Structure-function studies on small heat shock protein oligomeric assembly and interaction with unfolded polypeptides. *J. Biol. Chem.* **272**, 24 646–24 656. (doi:10.1074/jbc.272.39.24646)

47. Quinlan RA, Moir RD, Stewart M. 1989 Expression in *Escherichia coli* of fragments of glial fibrillary acidic protein: characterization, assembly properties and paracrystal formation. *J. Cell Sci.* **93**, 71–83.

48. Huiatt TW, Robson RM, Arakawa N, Stromer MH. 1980 Desmin from avian smooth muscle. Purification and partial characterization. *J. Biol. Chem.* **255**, 6981–6989.

49. Geisler N, Weber K. 1980 Purification of smooth-muscle desmin and a protein-chemical comparison of desmins from chicken gizzard and hog stomach. *Eur. J. Biochem.* **111**, 425–433. (doi:10.1111/j.1432-1033.1980.tb04957.x)

50. Owens DW *et al*. 2004 Human keratin 8 mutations that disturb filament assembly observed in inflammatory bowel disease patients. *J. Cell Sci.* **117**, 1989–1999. (doi:10.1242/jcs.01043)

51. Perng MD, Cairns L, van den IJssel P, Prescott A, Hutcheson AM, Quinlan RA. 1999 Intermediate filament interactions can be altered by HSP27 and alphaB-crystallin. *J. Cell Sci.* **112**, 2099–2112.

52. Houck SA, Landsbury A, Clark JI, Quinlan RA. 2011 Multiple sites in αB-crystallin modulate its interactions with desmin filaments assembled *in vitro*. *PLoS ONE* **6**, e25859. (doi:10.1371/journal.pone.0025859)

53. Atakhorrami M, Sulkowska JI, Addas KM, Koenderink GH, Tang JX, Levine AJ, MacKintosh F, Schmidt C. 2006 Correlated fluctuations of microparticles in viscoelastic solutions: quantitative measurement of material properties by microrheology in the presence of optical traps. *Phys. Rev. E Stat. Nonlinear Soft Matter Phys.* **73**, 061501. (doi:10.1103/PhysRevE.73.061501)

54. Addas KM, Schmidt CF, Tang JX. 2004 Microrheology of solutions of semiflexible biopolymer filaments using laser tweezers interferometry. *Phys. Rev. E Stat. Nonlinear Soft Matter Phys.* **70**, 021503. (doi:10.1103/PhysRevE.70.021503)

55. Myszka DG. 1999 Improving biosensor analysis. *J. Mol. Recognit.* **12**, 279–284. (doi:10.1002/(SICI)1099-1352(199909/10)12:5<279::AID-JMR473>3.0.CO;2-3)

56. Tholozan FM, Gribbon C, Li Z, Goldberg MW, Prescott AR, McKie N, Quinlan RA. 2007 FGF-2 release from the lens capsule by MMP-2 maintains lens epithelial cell viability. *Mol. Biol. Cell* **18**, 4222–4231. (doi:10.1091/mbc.E06-05-0416)

57. Sambrook J, Fritsch EF, Maniatis T. 1989 *Molecular cloning: a laboratory manual*. New York, NY: Cold Spring Harbor Press.

58. Perng MD, Wen SF, Gibbon T, Middeldorp J, Sluijs JA, Hol EM, Quinlan RA. 2008 GFAP filaments can tolerate the incorporation of assembly-compromised GFAP-δ, but with consequences for filament organization and αB-crystallin association. *Mol. Biol. Cell* **19**, 4521–4533. (doi:10.1091/mbc.E08-03-0284)

59. King RJ, Finley JR, Coffer AI, Millis RR, Rubens RD. 1987 Characterization and biological relevance of a 29-kDa, oestrogen receptor-related protein. *J. Steroid Biochem.* **27**, 471–475. (doi:10.1016/0022-4731(87)90342-6)

60. Sawada K, Agata K, Yoshiki A, Eguchi G. 1993 A set of anti-crystallin monoclonal-antibodies for detecting lens specificities—beta-crystallin as a specific marker for detecting lentoidogenesis in cultures of chicken lens epithelial-cells. *Jpn J. Ophthalmol.* **37**, 355–368.

61. Haley DA, Bova MP, Huang QL, McHaourab HS, Stewart PL. 2000 Small heat-shock protein structures reveal a continuum from symmetric to variable assemblies. *J. Mol. Biol.* **298**, 261–272. (doi:10.1006/jmbi.2000.3657)

62. Leroux MR, Ma BJ, Batelier G, Melki R, Candido EP. 1997 Unique structural features of a novel class of small heat shock proteins. *J. Biol. Chem.* **272**, 12 847–12 853. (doi:10.1074/jbc.272.19.12847)

63. Karabinos A, Schmidt H, Harborth J, Schnabel R, Weber K. 2001 Essential roles for four cytoplasmic intermediate filament proteins in *Caenorhabditis elegans* development. *Proc. Natl Acad. Sci. USA* **98**, 7863–7868. (doi:10.1073/pnas.121169998)

64. Gustavsson N, Kokke BP, Anzelius B, Boelens WC, Sundby C. 2001 Substitution of conserved methionines by leucines in chloroplast small heat shock protein results in loss of redox-response but retained chaperone-like activity. *Protein Sci.* **10**, 1785–1793. (doi:10.1110/ps.11301)

65. Kato K, Goto S, Inaguma Y, Hasegawa K, Morishita R, Asano T. 1994 Purification and characterization of a 20-kDa protein that is highly homologous to alpha B crystallin. *J. Biol. Chem.* **269**, 15 302–15 309.

66. Bukach OV, Glukhova AE, Seit-Nebi AS, Gusev NB. 2009 Heterooligomeric complexes formed by human small heat shock proteins HspB1 (Hsp27) and HspB6 (Hsp20). *Biochim. Biophys. Acta* **1794**, 486–495. (doi:10.1016/j.bbapap.2008.11.010)

67. Chou RG, Stromer MH, Robson RM, Huiatt TW. 1990 Determination of the critical concentration required for desmin assembly. *Biochem. J.* **272**, 139–145.

68. Mucke N, Wedig T, Burer A, Marekov LN, Steinert PM, Langowski J, Aebi U, Herrmann H. 2004 Molecular and biophysical characterization of assembly-starter units of human vimentin. *J. Mol. Biol.* **340**, 97–114. (doi:10.1016/j.jmb.2004.04.039)

69. Portet S, Mucke N, Kirmse R, Langowski J, Beil M, Herrmann H. 2009 Vimentin intermediate filament formation: *in vitro* measurement and mathematical modeling of the filament length distribution during assembly. *Langmuir* **25**, 8817–8823. (doi:10.1021/la900509r)

70. Yang ZW, Kong CF, Babitch JA. 1988 Characterization and location of divalent cation binding sites in bovine glial fibrillary acidic protein. *Biochemistry* **27**, 7045–7050. (doi:10.1021/bi00418a056)

71. Baldwin AJ, Lioe H, Robinson CV, Kay LE, Benesch JL. 2011 αB-crystallin polydispersity is a consequence of unbiased quaternary dynamics. *J. Mol. Biol.* **413**, 297–309. (doi:10.1016/j.jmb.2011.07.016)

72. Liu L, Ghosh JG, Clark JI, Jiang S. 2006 Studies of αB crystallin subunit dynamics by surface plasmon resonance. *Anal. Biochem.* **350**, 186–195. (doi:10.1016/j.ab.2005.12.019)

73. Hu WF *et al*. 2012 αA- and αB-crystallins interact with caspase-3 and Bax to guard mouse lens development. *Curr. Mol. Med.* **12**, 177–187. (doi:10.2174/156652412798889036)

74. Sathish HA, Stein RA, Yang G, McHaourab HS. 2003 Mechanism of chaperone function in small heat-shock proteins. Fluorescence studies of the conformations of T4 lysozyme bound to αB-crystallin. *J. Biol. Chem.* **278**, 44 214–44 221. (doi:10.1074/jbc.M307578200)

75. Claxton DP, Zou P, McHaourab HS. 2008 Structure and orientation of T4 lysozyme bound to the small heat shock protein α-crystallin. *J. Mol. Biol.* **375**, 1026–1039. (doi:10.1016/j.jmb.2007.11.014)

76. Ghosh JG, Shenoy Jr AK, Clark JI. 2007 Interactions between important regulatory proteins and human alphaB crystallin. *Biochemistry* **46**, 6308–6317. (doi:10.1021/bi700149h)

77. McDonald ET, Bortolus M, Koteiche HA, McHaourab HS. 2012 Sequence, structure, and dynamic determinants of Hsp27 (HspB1) equilibrium dissociation are encoded by the N-terminal domain. *Biochemistry* **51**, 1257–1268. (doi:10.1021/bi2017624)

78. Qin Z, Kreplak L, Buehler MJ. 2009 Hierarchical structure controls nanomechanical properties of vimentin intermediate filaments. *PLoS ONE* **4**, e7294. (doi:10.1371/journal.pone.0007294)

79. Franke WW, Schmid E, Wellsteed J, Grund C, Gigi O, Geiger B. 1983 Change of cytokeratin filament organisation during the cell cycle: selective masking of an immunologic determinant in interphase PtK2 cells. *J. Cell Biol.* **97**, 1255–1260. (doi:10.1083/jcb.97.4.1255)

80. Franke WW, Grund C, Kuhn C, Lehto V-P, Virtanen I. 1984 Transient change of organisation of vimentin filaments during mitosis as demonstrated by a monoclonal antibody. *Exp. Cell Res.* **154**, 567–580. (doi:10.1016/0014-4827(84)90181-2)

81. Snider NT, Weerasinghe SV, Iniguez-Lluhi JA, Herrmann H, Omary MB. 2011 Keratin hypersumoylation alters filament dynamics and is a marker for human liver disease and keratin mutation. *J. Biol. Chem.* **286**, 2273–2284. (doi:10.1074/jbc.M110.171314)

82. Hyder CL, Isoniemi KO, Torvaldson ES, Eriksson JE. 2011 Insights into intermediate filament regulation from development to ageing. *J. Cell Sci.* **124**, 1363–1372. (doi:10.1242/jcs.041244)

83. Icenogle LM, Hengel SM, Coye LH, Streifel A, Collins CM, Goodlett DR, Moseley SL. 2012 Molecular and biological characterization of streptococcal SpyA-mediated ADP-ribosylation of intermediate filament protein vimentin. *J. Biol. Chem.* **287**, 21 481–21 491. (doi:10.1074/jbc.M112.370791)

84. Korolainen MA, Auriola S, Nyman TA, Alafuzoff I, Pirttila T. 2005 Proteomic analysis of glial fibrillary acidic protein in Alzheimer's disease and aging brain. *Neurobiol. Dis.* **20**, 858–870. (doi:10.1016/j.nbd.2005.05.021)

85. Kueper T *et al*. 2007 Vimentin is the specific target in skin glycation. Structural prerequisites, functional consequences, and role in skin aging. *J. Biol. Chem.* **282**, 23 427–23 436. (doi:10.1074/jbc.M7015 86200)

86. Yuan J, Huiatt TW, Liao CX, Robson RM, Graves DJ. 1999 The effects of mono-ADP-ribosylation on desmin assembly-disassembly. *Arch. Biochem. Biophys.* **363**, 314–322. (doi:10.1006/abbi.1998.1096)

87. Hyder CL, Pallari HM, Kochin V, Eriksson JE. 2008 Providing cellular signposts—post-translational modifications of intermediate filaments. *FEBS Lett.* **582**, 2140–2148. (doi:10.1016/j.febslet.2008.04.064)

88. Der Perng M, Su M, Wen SF, Li R, Gibbon T, Prescott AR, Brenner M, Quinlan RA. 2006 The Alexander disease-causing glial fibrillary acidic protein mutant, R416W, accumulates into Rosenthal fibers by a pathway that involves filament aggregation and the association of αB-crystallin and HSP27. *Am. J. Hum. Genet.* **79**, 197–213. (doi:10.1086/504411)

89. Schopferer M, Bar H, Hochstein B, Sharma S, Mucke N, Herrmann H, Willenbacher N. 2009 Desmin and vimentin intermediate filament networks: their viscoelastic properties investigated by mechanical rheometry. *J. Mol. Biol.* **388**, 133–143. (doi:10.1016/j.jmb.2009.03.005)

90. Lin YC, Broedersz CP, Rowat AC, Wedig T, Herrmann H, Mackintosh FC, Weitz DA. 2010 Divalent cations crosslink vimentin intermediate filament tail domains to regulate network mechanics. *J. Mol. Biol.* **399**, 637–644. (doi:10.1016/j.jmb.2010.04.054)

91. Beck R, Deek J, Jones JB, Safinya CR. 2010 Gel-expanded to gel-condensed transition in neurofilament networks revealed by direct force measurements. *Nat. Mater.* **9**, 40–46. (doi:10.1038/nmat2566)

92. Kwon HJ, Kakugo A, Shikinaka K, Osada Y, Gong JP. 2005 Morphology of actin assemblies in response to polycation and salts. *Biomacromolecules* **6**, 3005–3009. (doi:10.1021/bm050320g)

93. Jones JB, Safinya CR. 2008 Interplay between liquid crystalline and isotropic gels in self-assembled neurofilament networks. *Biophys. J.* **95**, 823–835. (doi:10.1529/biophysj.107.127415)

94. Bennardini F, Wrzosek A, Chiesi M. 1992 αB-crystallin in cardiac tissue. Association with actin and desmin filaments. *Circ. Res.* **71**, 288–294. (doi:10.1161/01.RES.71.2.288)

95. Marcinek DJ, Kushmerick MJ, Conley KE. 2010 Lactic acidosis *in vivo*: testing the link between lactate generation and H+ accumulation in ischemic mouse muscle. *J. Appl. Physiol.* **108**, 1479–1486. (doi:10.1152/japplphysiol.01189.2009)

96. Golenhofen N, Ness W, Koob R, Htun P, Schaper W, Drenckhahn D. 1998 Ischemia-induced phosphorylation and translocation of stress protein αB-crystallin to Z lines of myocardium. *Am. J. Physiol.* **274**, H1457–H1464.

97. Golenhofen N, Perng MD, Quinlan RA, Drenckhahn D. 2004 Comparison of the small heat shock proteins αB-crystallin, MKBP, HSP25, HSP20, and cvHSP in heart and skeletal muscle. *Histochem. Cell Biol.* **122**, 415–425. (doi:10.1007/s00418-004-0711-z)

98. Jehle S *et al*. 2010 Solid-state NMR and SAXS studies provide a structural basis for the activation of αB-crystallin oligomers. *Nat. Struct. Mol. Biol.* **17**, 1037–1042. (doi:10.1038/nsmb.1891)

99. Jehle S *et al*. 2009 αB-crystallin: a hybrid solid-state/solution-state NMR investigation reveals structural aspects of the heterogeneous oligomer. *J. Mol. Biol.* **385**, 1481–1497. (doi:10.1016/j.jmb.2008.10.097)

100. Ghosh JG, Shenoy Jr AK, Clark JI. 2006 N- and C-Terminal motifs in human αB crystallin play an important role in the recognition, selection, and solubilization of substrates. *Biochemistry* **45**, 13 847–13 854. (doi:10.1021/bi061471m)

101. Bagneris C, Bateman OA, Naylor CE, Cronin N, Boelens WC, Keep NH, Slingsby C. 2009 Crystal structures of α-crystallin domain dimers of αB-crystallin and Hsp20. *J. Mol. Biol.* **392**, 1242–1252. (doi:10.1016/j.jmb.2009.07.069)

102. Hayes VH, Devlin G, Quinlan RA. 2008 Truncation of αB-crystallin by the myopathy-causing Q151X mutation significantly destabilizes the protein leading to aggregate formation in transfected cells. *J. Biol. Chem.* **283**, 10 500–10 512. (doi:10.1074/jbc.M706453200)

103. Lovicu FJ, Schulz MW, Hales AM, Vincent LN, Overbeek PA, Chamberlain CG, McAvoy JW. 2002 TGFβ induces morphological and molecular changes similar to human anterior subcapsular cataract. *Br. J. Ophthalmol.* **86**, 220–226. (doi:10.1136/bjo.86.2.220)

104. Chen Q *et al*. 2005 Intrasarcoplasmic amyloidosis impairs proteolytic function of proteasomes in cardiomyocytes by compromising substrate uptake. *Circ. Res.* **97**, 1018–1026. (doi:10.1161/01.RES.0000189262.92896.0b)

105. Pattison JS, Osinska H, Robbins J. 2011 Atg7 induces basal autophagy and rescues autophagic deficiency in CryABR120G cardiomyocytes. *Circ. Res.* **109**, 151–160. (doi:10.1161/CIRCRESAHA.110.237339)

106. Tannous P *et al*. 2008 Autophagy is an adaptive response in desmin-related cardiomyopathy. *Proc. Natl Acad. Sci. USA* **105**, 9745–9750. (doi:10.1073/pnas.0706802105)